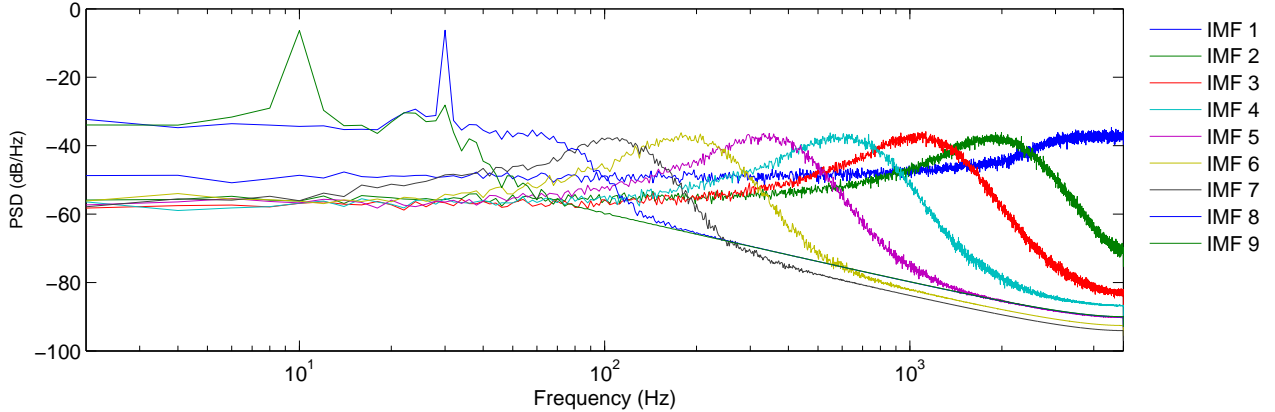


## 1 IMF spectra obtained using APIT-MEMD in Section 2.(a)



**Supplementary Figure 1: Averaged power spectral density (PSD) of the IMFs 1-9 of the fourth channel obtained using APIT-MEMD** The PSDs were averaged over 30 realisations, where SNR of the fourth channel was 0 dB, and the number of direction vectors 32.

Supplementary Figure 1 shows the averaged spectra of the IMFs 1-9 of the fourth channel obtained using APIT-MEMD in Section 2.(a). Observe that IMF indices 8 and 9 contained respectively the 10 Hz ( $f_1$ ) and 30 hz ( $f_2$ ) oscillations.

## 2 Noise assisted signal decomposition

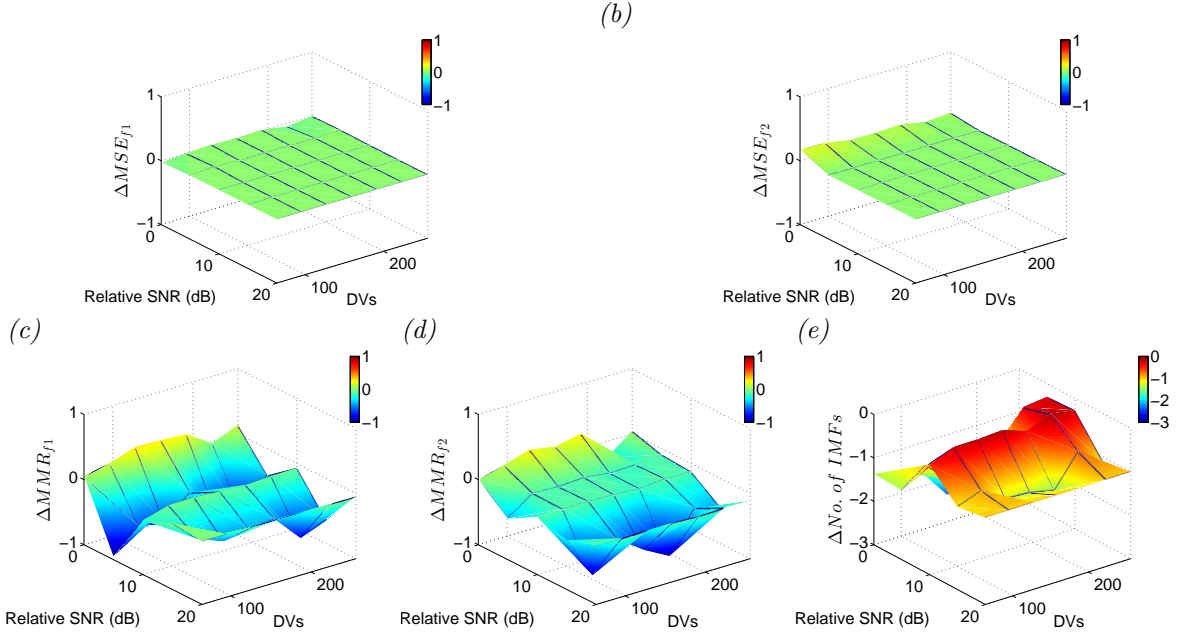
In this section the performance of the proposed APIT-MEMD algorithm in a noise-assisted mode of operation was evaluated against MEMD. Both algorithms were employed to decompose 3-channel data, augmented with 5 adjacent WGN channels, where the 3-channel data was composed of sinusoids given by

$$\begin{aligned} x_1(t) &= \cos(2\pi f_1 t) + \cos(2\pi f_2 t), \\ x_2(t) &= \sin(2\pi f_2 t), \\ x_3(t) &= \sin(2\pi f_1 t), \end{aligned} \tag{1}$$

where  $f_1=10$  Hz,  $f_2=30$  Hz, the sampling frequency  $f_s=10$  kHz, while the channels 4 to 8 were WGN processes with constant power. The SNRs of the 3-channel data relative to the noise channels were varied from 0 to 20 dB. The  $\alpha$  value for the NA-APIT-MEMD was 1. Supplementary Figure 2 (a-b) shows the differences in MSE in reconstructing the  $f_1$  and  $f_2$  oscillations using NA-APIT-MEMD and NA-MEMD. Supplementary Figure 2 (c-d) show the differences in MMR in reconstructing the  $f_1$  and  $f_2$  oscillations using NA-APIT-MEMD and NA-MEMD. Supplementary Figure 2 (e) shows the differences in the number of IMFs generated by the proposed NA-APIT-MEMD and NA-MEMD. All the results were obtained by averaging over 30 independent realisations. It can be seen that the performance of the proposed algorithm in terms of the MSE was comparable to that of NA-MEMD. The proposed algorithm, however, yielded lower MMR than NA-MEMD in the presence of power imbalances between the signal and noise channels (relative SNR > 5 dB), and consistently generated fewer IMFs. Supplementary Figure 3 shows the averaged spectra of the IMFs 1-8 of the fourth channel obtained using NA-APIT-MEMD.

## 3 P300 reconstruction

Supplementary Figure 4 shows the P300 ground truths for each of the 6 electrodes constructed using NA-APIT-MEMD and NA-MEMD.

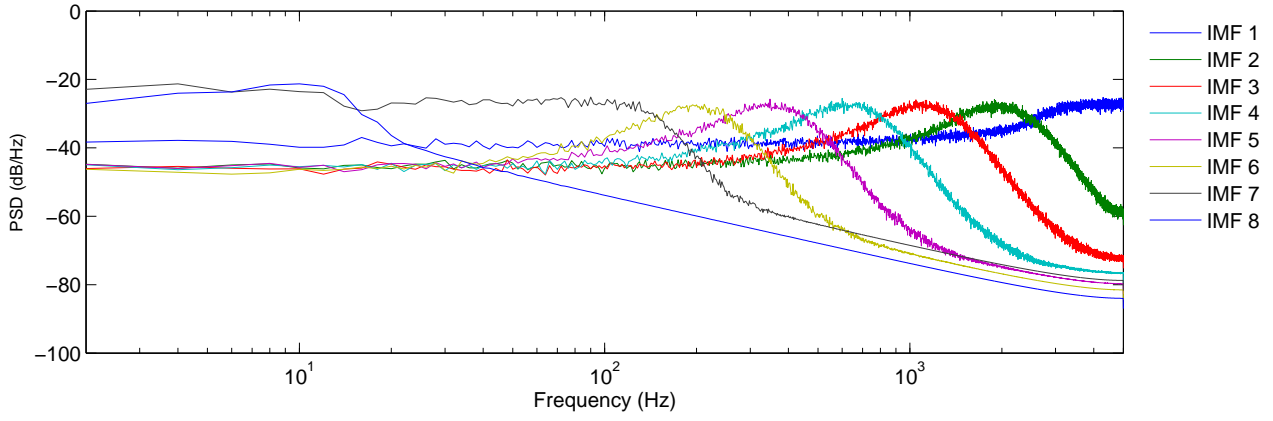


**Supplementary Figure 2: Performance comparison between APIT-MEMD and MEMD in reconstructing signal with the assistance of noise.** All performance measures follow the format: "APIT-MEMD – MEMD". (a): Difference in MSE in reconstructing the  $f_1$  sinusoid. (b): Difference in MSE in reconstructing the  $f_2$  sinusoid. (c): Difference in MMR in reconstructing the  $f_1$  sinusoid. (d): Difference in MMR in reconstructing the  $f_2$  sinusoid. (e): Difference in the number of IMFs.

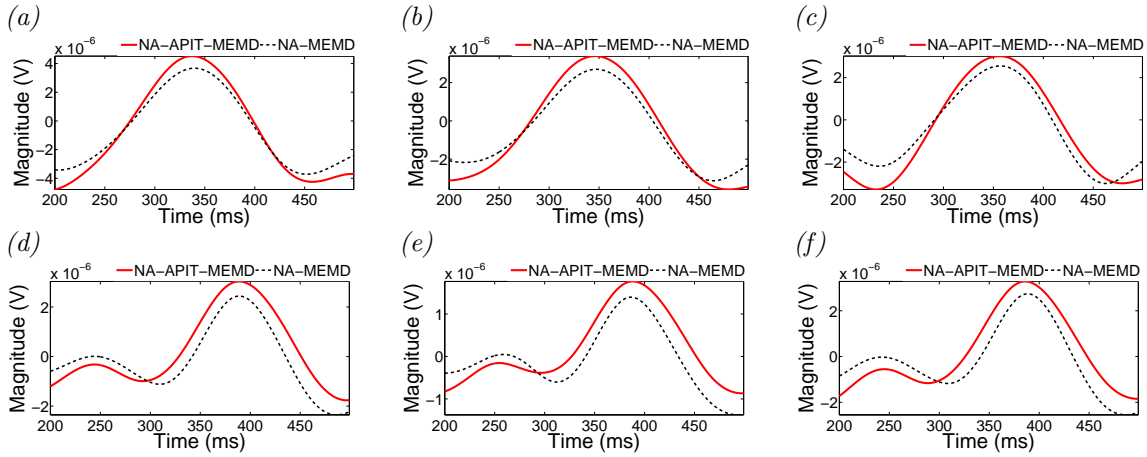
## 4 Differentiating between SSVEP responses at different frequencies

SSVEP responses of 50 seconds in length were recorded from two subjects seated next to each other and attending different SSVEP stimuli presented on an LCD screen. Subject 1 ( $y_1$ ) attended a 13-Hz SSVEP stimulus ( $s_1$ ), while subject 2 ( $y_2$ ) attended a 15-Hz SSVEP stimulus ( $s_2$ ). The recorded signals were then band-pass filtered to the range 10-20 Hz. Following the standard approach to phase synchrony estimation, PSI between each of the two stimuli ( $s_1$  and  $s_2$ , see Supplementary Figure 5 (a) and (b)), and each of the responses ( $y_1$  and  $y_2$ , see Supplementary Figure 5 (c) and (d)) was then estimated, and shown in Supplementary Figure 6 (a). Next, within our intrinsic multiscale analysis approach, the stimuli and responses ( $s_1$ ,  $s_2$ ,  $y_1$  and  $y_2$ ) were used to form 4-channel data and then decomposed using NA-APIT-MEMD with 10 adjacent WGN channels. The IMF with maximum power was then treated as the information-bearing IMF (IMF containing the required 13 Hz or 15 Hz oscillation). The PSIs between each of the information-bearing IMFs of the stimuli and responses were then calculated from 30 realisations of NA-APIT-MEMD, and shown in Supplementary Figure 6 (b).

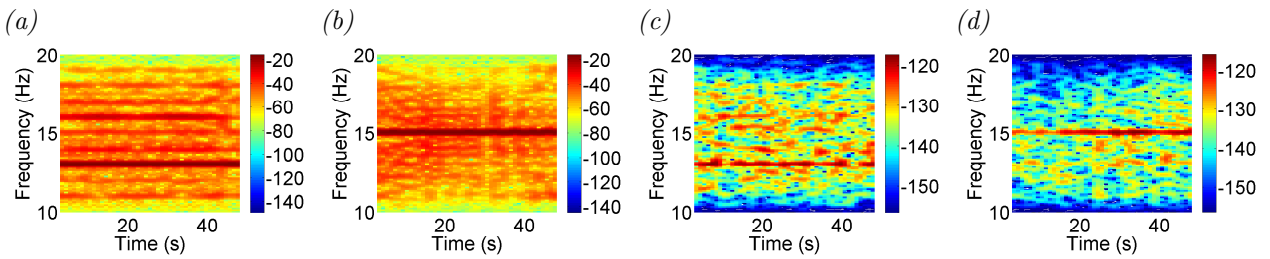
It can be observed from Supplementary Figure 6 (a) that, by using the standard approach, PSI between  $y_1$  and its corresponding stimulus,  $s_1$ , was lower than PSI between  $y_1$  and the non-corresponding stimulus,  $s_2$ , while in Supplementary Figure 6 (b) PSI estimated using the intrinsic multiscale analysis approach between the responses and corresponding stimuli ( $y_1$ - $s_1$  and  $y_2$ - $s_2$ ) were all significantly higher than all of the other PSIs, determined by the Z-test at a significance level of 0.05. This illustrates the efficacy of the intrinsic multiscale analysis in revealing phase relationship between SSVEP stimuli and responses.



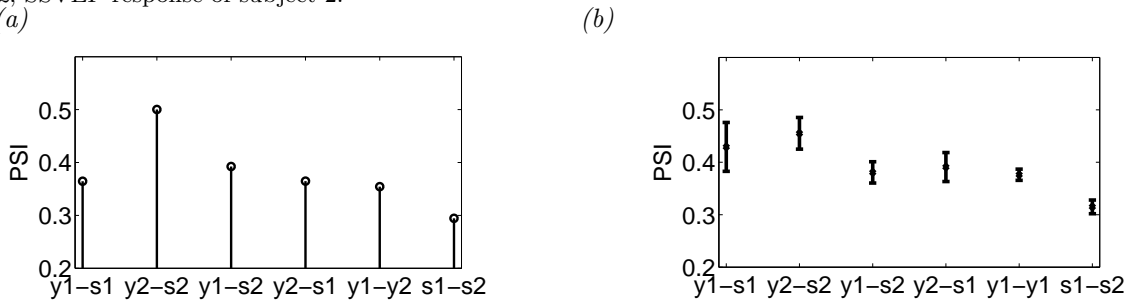
**Supplementary Figure 3: Averaged power spectral density (PSD) of the IMFs 1-9 of the fourth channel obtained using NA-APIT-MEMD** The PSDs were averaged over 30 realisations, where SNR of the fourth channel was 10 dB, and the number of direction vectors 32.



**Supplementary Figure 4: P300 ground truth generated by performing NA-APIT-MEMD and NA-MEMD on EEG data from two subjects at different electrode positions.** (a): Subject 1, Fz electrode. (b): Subject 1, Cz electrode. (c): Subject 1, Pz electrode. (d): Subject 2, Fz electrode. (e): Subject 2, POz electrode. (f): Subject 2, Oz electrode.



**Supplementary Figure 5: Spectrogram of SSVEP stimuli and brain responses.** (a):  $s1$ , 13 Hz SSVEP stimulus presented to subject 1. (b):  $s2$ , 15 Hz SSVEP stimulus presented to subject 2. (c):  $y1$ , SSVEP response of subject 1. (d):  $y2$ , SSVEP response of subject 2.



**Supplementary Figure 6: Estimated PSI between SSVEP stimuli and brain responses.** (a): PSI estimated using the standard approach. (b): PSI estimated using the intrinsic multiscale analysis.